Astronomy & Astrophysics manuscript no.
(will be inserted by hand later)

The EUV helium spectrum in the quiet Sun: a by-product of coronal emission?

Vincenzo Andretta[1], Giulio Del Zanna[2], and Stuart D. Jordan[3]

[1] Istituto Nazionale di Astrofisica/Osservatorio Astronomico di Capodimonte – Salita Moiariello, 16 – I-80131 Napoli – Italy
[2] Department of Applied Mathematics and Theoretical Physics – University of Cambridge – Cambridge – UK
[3] NASA's Goddard Space Flight Center – Laboratory for Astronomy and Solar Physics – Code 682 – Greenbelt, 20771 MD – USA

Received 00/00/0000 / Accepted 00/00/0000

Abstract. In this paper we test one of the mechanisms proposed to explain the intensities and other observed properties of the solar helium spectrum, and in particular of its Extreme-Ultraviolet (EUV) resonance lines. The so-called Photoionisation-Recombination (P-R) mechanism involves photoionisation of helium atoms and ions by EUV coronal radiation, followed by recombination cascades. We present calibrated measurements of EUV flux obtained with the two CDS spectrometers on board SOHO, in quiescent solar regions. We were able to obtain an essentially complete estimate of the total photoionising flux in the wavelength range below 504 Å (the photoionisation threshold for He I), as well as simultaneous measurements with the same instruments of the intensities of the strongest EUV helium lines: He II λ304, He I λ584, and He I λ537. We find that there are not enough EUV photons to account for the observed helium line intensities. More specifically, we conclude that He II intensities cannot be explained by the P-R mechanism. Our results, however, leave open the possibility that the He I spectrum could be formed by the P-R mechanism, with the He II λ304 line as a significant photoionisating source.

Key words. Radiative Transfer — Line: formation — Sun: chromosphere — Sun: corona — Sun: UV radiation

1. A brief historical overview of the problem

The question of how the helium lines are formed in the Sun has been with us since their discovery. Since helium is the second most abundant element in the Sun, and because of its apparently different fractional abundance in different regions of the solar atmosphere, especially if we include the solar wind, understanding the formation of its spectrum is of fundamental importance. In this paper we concentrate on the formation of the EUV spectrum in the quiet Sun, relying for this analysis on observations made with the Solar and Heliospheric Observatory (SOHO: Domingo et al. 1995). The particular question we address is what are the relative contributions of two long-studied processes known to be dominant (one, the other, or both working together) in forming the strong helium resonance lines, especially the He I λ584 line and the He II λ304 line. The two competing processes are direct collisional excitation of the line (possibly enhanced by non-thermal effects; see below), which immediately produces a photon because of the large Einstein coefficient for a principal resonance line, and photoionisation followed by recombination to the upper level of the line (either directly or in a cascade through intermediate levels). We call this latter process P-R, for Photoionisation-Recombination.

A good review of the overall problem prior to the 1990's is found in Zirin (1988). Zirin reviewed a large body of evidence from both ground-based visible and radio as well as space-based EUV observations in an effort to obtain a self-consistent picture of how all the solar helium lines are formed. In doing so, he concluded that the evidence favored the P-R mechanism for their formation. Coronal radiation was identified as the source of the required, comparatively high-energy photons short of the ionisation limits of He I and He II (504 Å and 228 Å respectively). However, while most authors supported this view for the visible or infrared lines of neutral helium, there was considerable controversy over the formation of the principal resonance lines in particular.

A good review of the alternative viewpoint, collisional excitation, in the same pre-1990s timeframe, was given by Athay (1988). In addition, C. Jordan (1975, 1980) noted that, if collisional excitation were the line formation mech-

Send offprint requests to: V. Andretta, e-mail: andretta@na.astro.it

anism of the principal resonance lines, their large excitation energy compared to their ionisation equilibrium temperature would make those lines very sensitive to nonthermal effects, such as non-maxwellian tails in the electron energy distributions. But C. Jordan also proposed that the large nonthermal velocities observed in the line-formation regions could greatly enhance the emergent intensity by exposing many of the ions to higher temperature thermal electrons if the temperature gradient is large, as in the solar Transition Region (TR). We call this process "velocity redistribution", V-R, but point out that it should not be confused with use of the similar term in radiative transfer studies of optically thick lines. If velocity redistribution does indeed work as proposed, it would resolve a large discrepancy between static-atmosphere, non-LTE calculations and observations from both Skylab and, more recently, SOHO (Macpherson & Jordan 1999), where the observed fluxes in the principal resonance lines greatly exceed those calculated values. However, it is important to note that this hypothesis is dependent upon collisional excitation dominating the line formation.

The problem prior to the 1990s was that observations were inadequate to resolve the issue for the EUV lines. Either the spatial resolution or the spectral resolution of the observations was insufficient to settle the issue, and simultaneous observations of the corresponding ionising radiation were generally lacking. With improved observations in the 1990s, the situation changed. The first mission to provide relatively high spatial and spectral resolution (5″ spatial and about 55 mÅ spectral) and at least a proxy for the photoionising radiation was the Goddard Solar Extreme Ultraviolet Research Telescope and Spectrograph (SERTS). Using data from the 1989 flight of SERTS, S. Jordan et al. (1993) concluded that collisional excitation mechanism was overwhelmingly dominant in the formation of the He II λ304 line in the quiet Sun and probably in weak active regions, but that the issue remained open in strong active regions. However, that conclusion was based on the assumption that the line would form near the temperature of maximum ionic abundance, $T_e > 50\,000$ K, as estimated by "standard" ionisation equilibrium calculations. But, as discussed in Sec. 2, in a pure P-R scenario the helium spectrum in general, and the He II λ304 line in particular, would form at much lower temperatures, where the collisional excitation rates would be dramatically reduced, and would therefore become much smaller than the photoionisation rates induced by EUV coronal radiation.

A further study using mainly SERTS data by Falconer et al. (1998) supported the conclusions of Jordan et al. (1993), but by then we had entered the SOHO era. Assuming that collisional excitation dominated the formation of the He II λ304 line, Andretta et al. (2000) combined observations from two SERTS flights with both SOHO and ground-based sources to assess the C. Jordan hypothesis of velocity redistribution described above. They concluded that this mechanism could at least partly explain the high observed intensity in the 304 Å line in the quiet Sun, making it even more critical to determine once and for all if collisional excitation is overwhelmingly dominant in that region.

As SOHO gave us for the first time the possibility of combining observations of fluxes in the principal resonance lines and continua of neutral and ionised helium, as well as excellent images of the 304 Å line to provide context, the study reported here was initiated. The methodology used in this study is discussed in detail in Sec. 2 and App. A, but was already applied in an embryonic form by Zirin (1975). In applying this methodology, it is important to stress that more than one formation mechanism may be at work in different regions of the atmosphere. Also, because of the large difference in optical thickness between the resonance lines and subordinate lines, the latter may easily be produced by the P-R process, even if the former are produced largely, or at least partly, by collisional excitation. An in-depth discussion of these issues, in the case of the He I spectrum, can be found in Andretta (1994) and Andretta & Jones (1997).

In any case, we emphasise that the question whether the P-R mechanism is dominant or not in the solar atmosphere, can have profound implications in the interpretation of the observations.

More specifically, as discussed more in detail in Sec. 2, if the P-R mechanism is the dominant excitation process, the formation of the helium spectrum will depend, apart from the photoionising source (the coronal EUV radiation), primarily upon the *density stratification* of the absorbing medium (the solar atmosphere), and much less upon its *temperature structure*. Taking into account the relevant cross-sections and typical quiet Sun chromospheric densities, we would in fact expect helium emission to take place in a narrow and relatively homogeneous layer in the upper chromosphere (see, e. g., Zirin 1988). Again, more detailed calculations (Andretta & Jones 1997) bear out such expectation.

Conversely, if P-R is not the dominant mechanism, the formation of the resonance helium spectrum will take place in a temperature region corresponding to the lower TR. Our understanding, then, of the formation of the helium spectrum would be intimately related to our understanding of the physics of the TR. Quite possibly, the helium spectrum could even provide important information on the structure and dynamics of that region.

Therefore, understanding the role of the P-R mechanism is an essential first step in building an interpretive framework for observed solar helium spectra and spectroheliograms. Only when this understanding is secure can we be sure in what regions and for what line(s) to apply the assumption of dominant collisional excitation to the solution of other outstanding problems in the formation of the helium resonance lines.

With this work, we intend to contribute to such understanding, at least as far as the quiescent solar atmosphere is concerned, by using a more direct approach (described in Sec. 2) than the indirect clues usually produced in the past. As described in Sec. 3, we have taken advantage of the exceptional wavelength coverage of the

SOHO EUV instruments, in particular of the Coronal Diagnostic Spectrometer (CDS, Harrison et al. 1995), while also exploiting the considerable level of accuracy and inter-consistency of their absolute intensity calibration. As demonstrated in the following sections, both a wide wavelength coverage and a reliable intensity calibration are essential for the test we carried out.

2. An approach to the problem

The EUV wavelength range of interest for the present discussion is shown in Fig. 1, together with the relevant photoionisation cross-sections. The wavelengths of the first members of the resonance series of helium and hydrogen are marked with solid vertical lines, together with the wavelengths of the corresponding continuum limits (dashed vertical lines). For ease of comparison, Fig. 1 also shows the first-order wavelength coverage of CDS. We also note that one of the filters of the the SOHO Extreme Ultraviolet Imaging Telescope (EIT, Delaboudinière et al. 1995) is centered on the He II λ304 line, while the other SOHO EUV spectrometer, SUMER (Wilhelm et al. 1995), is capable of observing the He I λ584 line in second order, as well as the several terms of the He II Balmer series.

The helium cross-sections plotted in Fig. 1 are per H atom, i. e. multiplied by the abundance of helium (we have adopted the photospheric value $n(\mathrm{He})/n(\mathrm{H}) = 0.085$). In Fig. 1 we show the measured He^0 cross-sections from West & Marr (1976), while the Gaunt factors for H and He^+ are from Karzas & Latter (1961).

In the inset we also show on a wider wavelength range the XUV opacity due to inner-shell photoabsorption by metals, again normalised to hydrogen and summed over all the elements Z for which cross-sections were available: $\sum_{\mathrm{Z}} \sigma_{\mathrm{Z}} \times (n(\mathrm{Z})/n(\mathrm{H}))$. In a neutral gas of photospheric composition, the total opacity is simply the sum of the latter component and the He^0 and H contributions (as in, e. g., McCammon & Morrison 1983). The cross sections data are from Henke et al. (1982) via the interpolation formulae of Bałucińska-Church & McCammon (1992); the set of photospheric abundances adopted is from Grevesse & Sauval (1998). In neutral media, Compton scattering, not shown here, becomes significant only above ~ 4 keV.

The comparison shown in Fig. 1 is obviously for illustrative purposes only: for a chromospheric plasma the relative ionic fractions of the two helium ions and the ionisation state of hydrogen need to be taken into account (see also Sec. 2.2); the same is true for the metal opacity, even though inner-shell cross sections vary little between neutrals and ions.

2.1. Basic assumptions

It is quite clear that coronal EUV radiation must induce a P-R effect in the solar atmosphere, at least to some extent. As mentioned in Sec. 1, in the quiet Sun coronal photons penetrate down to the upper chromosphere, where a narrow helium emission layer is formed. We can call this layer the "P-R layer", the analogue of a Chapman (1931) absorption layer in the Earth's ionosphere.

In this relatively cool region ($T_{\mathrm{e}} < 10^4$ K), collisions are very inefficient in populating the excited levels of helium atoms and ions, at energies greater respectively than ~ 20 and 40 eV from the ground level. Therefore we can assume that all helium resonance photons created in a P-R layer are the result of the recombination of an electron with a helium ion or alpha particle, following photoionisation by a EUV photon. In fact, this assumption works well in the quiescent atmosphere. However, it should be noted that in denser regions (e. g. active regions), coronal photons may be absorbed in shallower, hotter layers of the atmosphere, where collisional ionisation/excitation processes may give a significant contribution.

Collisional excitation processes in hotter layers of the atmosphere might add to this radiatively excited component (even though their simple additivity is not guaranteed, e. g.: Andretta & Jones 1997). The hypothesis we want to test in this paper, however, is that coronal radiation, via the P-R mechanism, is the *sole* significant source of excitation of helium resonance lines and continua in the quiet Sun.

In this case, we expect that the flux of coronal EUV photons (at $\lambda < 504$ Å) impinging on the chromosphere must be equal to, or greater than the flux of helium resonance (lines and continua) photons from the P-R layer. Thus:

$$\Phi^{\mathrm{res}}[\mathrm{He\,I}] + \Phi^{\mathrm{res}}[\mathrm{He\,II}] < \Phi^{\mathrm{cor}}[\lambda < 504]. \quad (1)$$

In the above inequality, $\Phi^{\mathrm{res}}[\mathrm{He\,I}]$ and $\Phi^{\mathrm{res}}[\mathrm{He\,II}]$ denote the total photon fluxes emerging from the atmosphere in the resonance series of He I (starting at 584 Å) and He II (starting at 304 Å), and from the resonance continua ($\lambda < 504$ Å for He I, and $\lambda < 228$ Å for He II). Similarly, the notation $\Phi^{\mathrm{cor}}[\lambda < 504]$ indicates the total incident flux from all the coronal lines shortwards 504 Å. These fluxes, $\Phi^{\mathrm{res}}[\mathrm{He}] \equiv \Phi^{\mathrm{res}}[\mathrm{He\,I}] + \Phi^{\mathrm{res}}[\mathrm{He\,II}]$ and $\Phi^{\mathrm{cor}}[\lambda < 504]$, coincide with Φ^{in} and Φ^{out}, respectively, in Fig. 2 and App. A, where a more formal derivation of Eq. 1 is discussed.

2.2. Some notes and caveats

It is important to note that the derivation of Eq. 1 rests on the assumption that the absorbing medium is not embedded in the source of photoionising radiation (so that we can evaluate "incoming" and "outgoing" fluxes at surface S': Fig. 2), and that all incident radiation is eventually absorbed (so that we can neglect flux at S'', as in the case of a semi-infinite atmosphere). Solar prominences, for example, may be physical instances when the application of Eq. 1 is likely not to be correct.

Eq. 1 gives equal weight to all photons capable of photoionising helium atoms and ions, whereas it would seem more intuitive to consider only those photons whose absorption cross-section is largest (photons near the photoionisation thresholds at 504 Å and 228 Å). Again, this is a consequence of the assumption of complete absorption

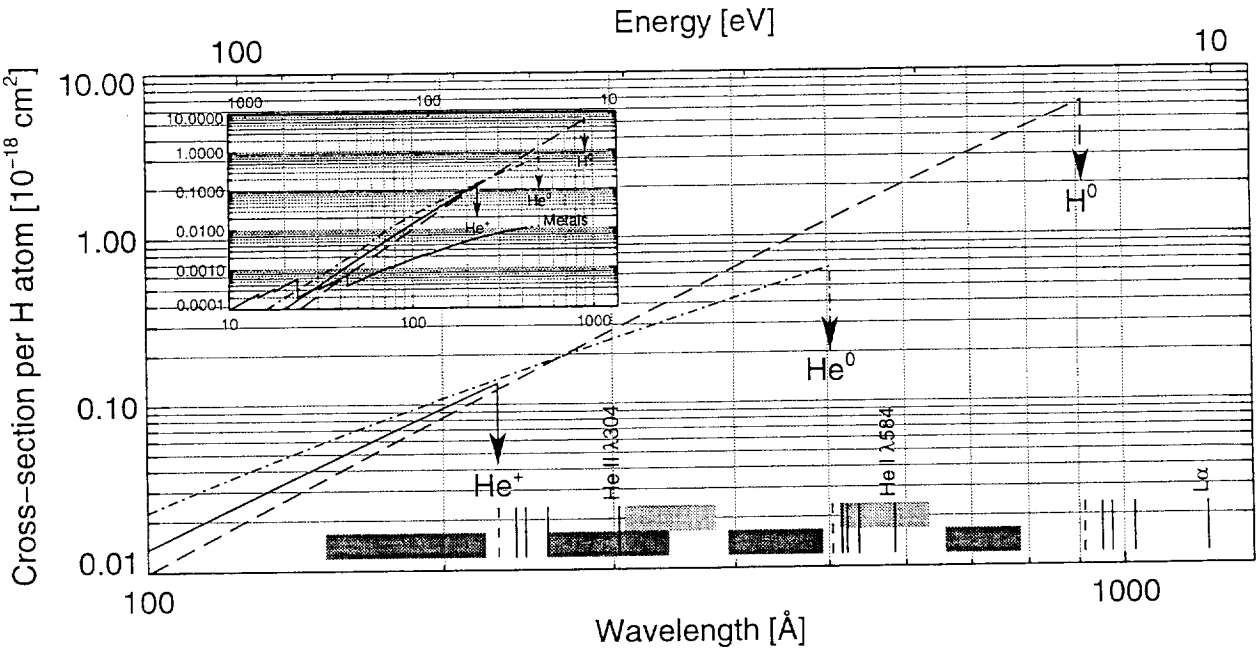

Fig. 1. Photoionisation cross sections for He^0 (dot-dashes), He^+ (solid) and H^0 (dashes), per hydrogen atom. In the inset, these cross sections are compared on a wider wavelength range to XUV photoabsorption by metals. Vertical lines at the bottom of the plot mark the wavelengths of the first resonance lines and of continuum edges for He and H; the gray areas indicate the wavelength coverage (first spectral order) of the two spectrometers of SOHO/CDS: Normal Incidence, NIS (lighter gray), and Grazing Incidence, GIS (darker gray).

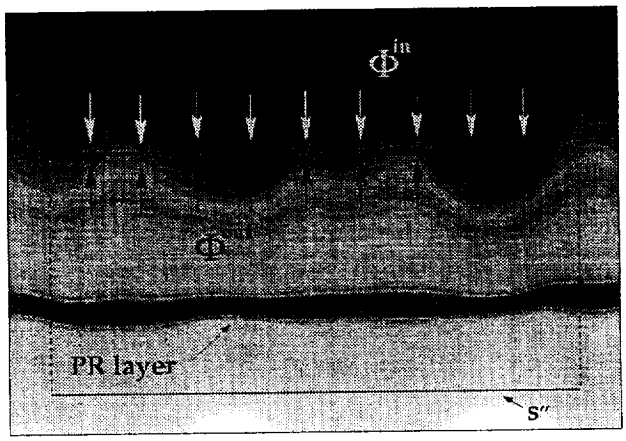

Fig. 2. Schematic geometry of the P-R mechanism in a semi-infinite, gravity-stratified atmosphere, discussed in Sec. 2 and App. A (density increasing towards the bottom of the sketch). The box enclosing a section of the P-R layer represents a cross section of surface S across which the photon flux of Eq. A.16 is to be evaluated. No physical or realistic scale is implied by this sketch, even though, as required in App. A, the vertical scale is to be considered much less than the horizontal size of S.

of incident radiation: a photon at 250 Å is 3.5 times less likely to be absorbed by a He^0 atom than one at 500 Å, but that only means it will travel further down (not very far, in a gravity-stratified atmosphere) before being absorbed and re-emitted, for instance in one of the resonance He I lines.

Another point worth stressing here is that not all collisional rates need to be negligible for Eq. 1 to be valid. In fact, de-excitation rates, which have a less steep dependence on temperature than direct excitation/ionisation from ground level, may be important even at relatively low temperatures. But their effect is to remove photons from the pool in the left-hand side of Eq. 1, increasing the unbalance between $\Phi^{\rm res}[{\rm He}]$ and $\Phi^{\rm cor}[\lambda < 504]$. This effect is enhanced by the presence of metastable levels, such as $He^0\ 1s2s\ ^3S$.

In obtaining Eq. 1, some assumptions were made regarding opacity and emissivity by other elements other than helium ("background" terms; see App. A). Beside helium, in the wavelength range we are considering the main absorber is hydrogen. For wavelengths below ~ 50 Å, absorption by inner-shell electrons of heavier elements may also become important (Fig. 1). A rough estimate of the role of H can be obtained by computing the ratio of cross-sections at 504 Å: $\sigma(He^0)/\sigma(H) = 6.1$; therefore, in a mostly-neutral plasma (and using the photospheric value $n({\rm He})/n({\rm H}) = 0.085$) more than a half of the photons at that wavelength would be absorbed by hydrogen. Of course, this estimate strongly depends on the relative ionisation state of H and He: a proper estimate of the effect of the opacity by hydrogen would therefore require detailed modeling (including non-LTE radiative transfer). But absorption by H is certainly an important effect, and

an effect that again goes in the direction of strenghtening the upper limit to helium emission given in Eq. 1.

Moreover, at the temperatures we are considering ($T < 10^4$ K), photons absorbed by hydrogen are most likely re-emitted beyond the He^0 limit: near the edge of the Lyman continuum (912 Å) – because of the dependence as $\exp(-h\nu/kT)$ of its emissivity – or in the other longer-wavelength lines or continua. These photons are thus lost, as far as the P-R mechanism is concerned. Furthermore, the relatively low temperature of the chromosphere ensures that emission processes other than due to H and He – emission in metallic lines, bremsstrahlung, two-photon decay from H-like ions – give a negligible contribution in the wavelength range $\lambda < 504$ Å (e. g.: Landini & Monsignori Fossi 1990). This justifies the assumption that the "background" emissivity is negligible in the range of interest.

2.3. Restricting the test to ionised helium only

In the derivation of the upper limit to helium emission of Eq. 1, all possible ways of redistributing photons among radiative transition of both He^0 and He^+ have been taken into account. Therefore, we were only able to place a constraint on the *sum* of the flux from the two ions. However, a closer inspection of the rate equations reveals that, in a P-R layer, the main mechanism of interaction between the two species occurs through the transition $He^0\ 1s^2 \longleftrightarrow 1s\ He^+$: He II resonance photons (e. g. He II λ304 or He II λ< 228) can photoionise He^0 atoms, and thus be converted in He I resonance photons, while, viceversa, photons in the resonance He I λ< 504 continuum can, in principle, photoionise/excite He^+ ions. It is easy to realise, however, that the latter process involves only the far tail of the He I recombination continuum: given the steep dependence on wavelength of its emissivity for the temperatures we are considering, this effect is negligible. Thus, if we restrict our treatment to He^+ ions only, we can treat He^0 atoms as another "background" absorber ("sink" of photons), exactly in the same fashion as we dealt with hydrogen.

In other words, if we make the approximation that there is no pumping of the He II resonance transitions by the He I continuum – but still allowing the reverse process, i. e. photoionisation of He I by He II radiation – we obtain:

$$\Phi^{\rm res}[\text{He II}] < \Phi^{\rm cor}[\lambda < 228]. \quad (2)$$

The upper limit to He II emission given in the latter inequality, together with the upper limit to the total He emission of Eq. 1, is the basis for the observational test on the "pure P-R" scenario we are about to describe.

3. The observational test

The null hypothesis we want to test, as stated in Sec. 2.1, is that the P-R mechanism is the only process producing the observed He emission in the quiet solar atmosphere. From an observational point of view, then, Eqs. 1 and 2 provide useful upper limits to the helium emission, with only rather weak constraints on the details of the geometry and of the transport of radiation.

No strong coronal lines overlap the main helium resonance lines: therefore, even observations with relatively modest spectral resolution would easily disentangle the photoionising radiation illuminating the chromosphere from helium emission. The only significant exception is a Si X line blended with He II λ256 (Thomas & Neupert 1994; Brosius et al. 1998), but their contribution to terms $\Phi^{\rm cor}[\lambda < 504]$ and $\Phi^{\rm res}[\text{He}]$, respectively, is however small (see also Sec. 3.1). Stronger observational requirements are, on the other hand, the full coverage of the range $\lambda < 584$ Å, and a reliable intensity calibration. The two CDS spectrometers are probably the instruments best suited for this test, as discussed below.

3.1. Rationale for using CDS

3.1.1. Wavelength coverage

The wavelength coverage of the Grazing Incidence Spectrometer (GIS) is sufficiently ample – covering most of the range 150–490 Å with its first three bands (Fig. 1) – to make it the best choice for estimating the total coronal flux impinging on the quiescent chromosphere, $\Phi^{\rm cor}[\lambda < 504]$. In Sec. 3.3 we will give an estimate of the quiet Sun coronal flux missing in GIS spectra, and show that the fluxes measured by GIS, $\Phi^{\rm cor}[\lambda < 504]$ and $\Phi^{\rm cor}[\lambda < 228]$, provide indeed a fairly complete count of the number of coronal photons below both the He^0 and He^+ photoionisation thresholds, respectively.

As far as He emission is concerned, $\Phi^{\rm res}[\text{He}]$, all the He II resonance series, except the He II λ304 line, unfortunately fall in the gap between GIS1 and GIS2. The He II λ256 line is not observable by GIS even in second-order spectra (falling in the gap between GIS3 and GIS4), in addition to being blended with a Si line, as mentioned earlier, which would have made its measure difficult at the GIS resolution anyway. The other higher-term lines could appear in second-order GIS3, but they are probably blended with other stronger lines, so no clear identification of those lines has been reported in quiet-Sun GIS spectra. The only He resonance line observable with GIS is therefore He II λ304. That indeed is a very prominent feature in the GIS2 band, but its very strength makes its absolute calibration very difficult, if not impossible. Finally, the egdes of the He I and He II continua are just beyond the spectral ranges of GIS1 and GIS3, respectively. It could be possible to measure the tail of those continua, but edge effects on the GIS detectors rule out this possibility, at least with the current knowledge of these detector effects.

The Normal Incidence Spectrometer (NIS) on the other hand, has a smaller wavelength coverage (often reduced by windowing, for telemetry reasons), but it can readily measure the first few lines of the resonance He I series, including the first and strongest term, the He I λ584 line, in the band NIS2 (Fig. 1). Moreover, the He II λ304

line is sufficiently strong (in fact the strongest line in the EUV spectrum of the quiet Sun) that it prominently appears in NIS2 second-order spectra.

While it can be argued that the NIS istrument can indeed give a reasonable complete estimate of the total photon flux in the He I resonance lines, it is true that the only He II emission line observable by CDS is the He II λ304 line. However, observations from pre-SOHO instruments (as summarised by Mango et al. 1978, for instance) give a ratio He II λ304/He II λ256 > 15. Thus, we expect that the He II λ304 line alone would give nearly all the total flux in He II resonance lines.

On the other hand, a rather large contribution to $\Phi^{\rm res}$[He] may come from the recombination continua. For typical chromospheric or TR temperatures, the recombination rate to the He^{+} ground level amounts to about 1/3 of the total recombinations from He^{++}. So, as already noted by Zirin (1975), while about 2/3 of the helium emission is in the form of resonance lines (mostly He II λ304), up to 1/3 of the photons may be in the recombination continuum below 228 Å. Similarly, around 1/2 of the recombinations to He^{0} are direct recombinations to the ground level. Data for the He I recombination continuum are given by Vernazza et al. (1981): fitting the tabulated intensities for their "C" ("average") quiet-Sun component in the range 470–504 Å with an exponential in frequency (i. e. assuming a constant color temperature), an integrated intensity of 9×10^{12} photons s^{-1} cm^{-2} sr^{-1} is obtained. On the other hand, Vernazza & Reeves (1978) give for their "average" quiet Sun the value of 1.6×10^{13} photons s^{-1} cm^{-2} sr^{-1} for the intensity of the He I λ584 line. Of course, a comparison between these numbers must be taken *cum grano salis*, but is indicative of the fact that the resonance continua can indeed give a significant contribution to the total EUV helium emission.

In short, while the precise value of the relative continuum/lines intensity ratio depends on the details of the transfer of radiation (mainly: geometry), it is reasonable to expect that the total photon flux in He lines measured with CDS may be lower than the total flux $\Phi^{\rm res}$[He] by a factor up to 2. This fact will be taken into account in the discussion of the results, in Sec. 3.4.

In summary, the two CDS detectors nicely complement each other in allowing estimates of the fluxes $\Phi^{\rm cor}[\lambda < 504]$ and $\Phi^{\rm res}$[He] required by Eqs. 1 and 2. The main operational difficulty consists in obtaining accurate cross-calibration between these two components of the CDS instrument, with special care on the second-order calibration of the NIS detector, essential for measuring the He II λ304 line.

3.1.2. Intensity calibration

There has been a good deal of work on the part of different groups, which has been steadily converging on a consistent absolute radiometric calibration of all the instruments onboard SOHO. This has been achieved with laboratory measurements, calibration rockets, and inter-calibration studies among the different SOHO instruments. Two SOHO inter-calibration workshops have taken place, which led to a publication on the subject (Huber et al. in press). Details on the CDS calibration and its improvements over the years can be found in Del Zanna et al. (2001). These authors also provide the first complete in-flight inter-calibration between all the 9 NIS and GIS channels (6 in first order and 3 in second) thereby bringing a significant update to the GIS absolute calibration, that turned out to be quite different from that one measured in laboratory. Del Zanna et al. (2001) based their relative calibration on the reference value at 584 Å derived by Brekke et al. (2000) with an inter-calibration between NIS and an EGS rocket flight launched in May 1997. Recently, the Brekke et al. (2000) work has been revised to take into account the effects on the NIS detector of the gain depression caused by exposures with the wide slit (Thompson 2001). The resulting new NIS calibration is similar to the previous one, but has a responsivity at 584 Å that is about 15% higher. This in turn results in a calibrated intensity of the 584 Å line that is 15% lower (and that is now in agreement, within the uncertainties, with the SUMER measurements).

In this paper we adopt the comprehensive calibration work of Del Zanna et al. (2001) but revise the absolute values to reach consistency with the new value at 584 Å (5.44×10^{-4} counts/photon). This in turn has the effect of increasing the second order responsivity at 304 Å to $1.56 \pm 0.4 \times 10^{-5}$.

For the NIS in second order, the EGS and the SERTS-97 (Thomas et al. 1999) rocket flights provided two measurements of the calibration at 304 Å. Both rockets were calibrated on the ground against primary standards, and produced similar values of the NIS responsivity (about 1.65×10^{-5} counts/photon). These results suffer from some uncertainties related to solar variability and the difficulty of spatial and temporal alignement with NIS. A revision of the SERTS-97 vs. NIS calibration is in progress (Thomas 2001). The effects of the NIS gain depression caused by exposures with the wide slit have recently been considered (Thompson 2001), providing new second order responsivities at 304 Å of 1.84 ± 0.4; $1.87 \pm 0.3 \times 10^{-5}$ (from the EGS and SERTS-97 data respectively). Note that these absolute values are slightly higher (15-20%) than the value adopted here. However, it is important to realize that for our test we only need a good cross-calibration between NIS and GIS. With the improvements in the work by Del Zanna et al. (2001), the accuracy of the relative NIS/GIS calibration is estimated to be around 20%. Within this uncertainty, all the recent studies on the CDS calibration are consistent.

3.2. The observations

The observations analysed here were taken during the period 7–13 May 1997 as part of a SOHO campaign explicitly

aimed at determining the role of the P-R mechanism in the quiet Sun, and within the framework of the SOHO Joint Observing Program (JOP[1]) #16. During this particular series of JOP16 observations, the CDS spectra were taken in coordination with another EUV SOHO spectrometer, SUMER, which provided information on the observed regions at higher temporal, spatial, and spectral resolution. A discussion of these SUMER data will be made in a follow-up study.

For planning reasons, the target region had to be selected one day prior to each observing sequence. Because of a problem in its scan mechanism, during the campaign the SUMER slit was fixed at approximately $X = +700''$ (SOHO coordinates), while still being free to move in the N-S direction. With this constraint, we tried to select quiescent regions which during the observations would be as far as possible from active regions. Fig. 3 summarises the locations observed during the campaign. The rectangular areas represents the Field-Of-View (FOV) of CDS/NIS and GIS, overlayed on one of the synoptic images taken on the same day with EIT.

The daily observing sequence for CDS consisted of alternating NIS and GIS observing programs, described below, scanning the target region. This approach minimises the effect of time variability on the total fluxes derived from the CDS spectra.

The NIS observing program used for these observations is identified by the acronym HECATRNS. This program uses the narrow slit, $2 \times 240''$, to image the target region with an E-to-W raster comprising 60 spectra taken at a step of $2''$: the total area covered is then $120 \times 240''$. The exposure time of each spectrum is of 46 s; the total duration of the raster, including overheads and data transmission, is normally $\sim$ 55 minutes (assuming a telemetry rate of 11.3 kbits/s). For telemetry reasons, data for only 14 windows of 21 pixels each in the dispersion direction were returned (4 in NIS1, and 10 in NIS2). Of these windows, three pairs were juxtaposed to cover broader multiplets or groups of lines, effectively bringing the number of windows to 11. The windows were selected to return the profiles of the first two He I resonance lines (at 584 Å and 537 Å) and the He II λ304 line (in second order spectrum), plus some strong TR and coronal lines for context.

The acronym identifying the GIS observing program is HECATRGS. The GIS detectors are SPAN (Spiral Anode) MCP (MicroChannel Plate) detectors, described in Breeveld et al. (1992) and Breeveld (1996). The specific set of on-board Look-Up Tables (LUTs) used to produce the pixel positions along the detectors for the raw data is identified by the parameter GSET_ID. For HECATRGS, GSET_ID=42. The slit used is the no. 2: $4 \times 4''$. The program comprises 200 spectra at 10 mirror (E-to-W) and 20 slit (S-to-N) positions, with a $4''$ step, for an overall

[1] SOHO JOPs provide the framework for maximising the coordination between SOHO instruments, and often involve collaborations with other ground-based or space-based observatories.

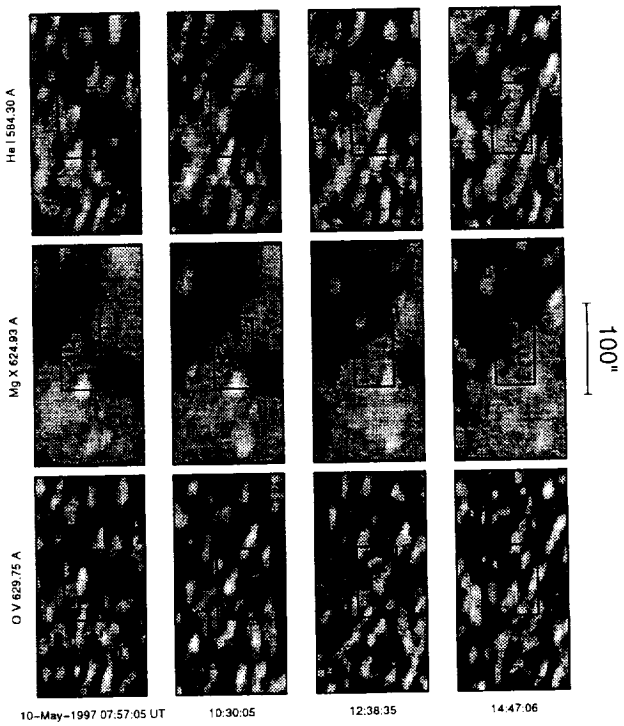

Fig. 4. Images obtained from selected lines in NIS spectra, for 4 raster of the 10 May sequence. The rectangles indicate the FOV of the interleaved GIS rasters, shifted taking into account solar rotation

area covered of $40 \times 80''$. The exposure time of each spectrum is 20 s. The total duration of the program, including overheads, is normally $\sim$ 74 minutes (if the appropriate LUTs need not to be loaded, and with the normal CDS telemetry rate).

In this work we choose to examine in detail the data taken on 7 and 10 May. The areas observed during these observing sequences cover quiescent areas of the Sun furthest away from active regions, at values of μ_c (cosine of the angle from disk center) of 0.66 and 0.64 respectively, at FOV center (Fig. 3). The data from 11 May are similar to the data taken on 10 May, except for a rather persistent brightening crossing the middle of the GIS FOV. We will briefly discuss intensities from this feature in Sec. 3.4.

3.3. Data analysis

Standard corrections were applied to the raw NIS data. They included de-biasing, flat-fielding, corrections for gain depression effects, cosmic ray removal. A few minor corrections were applied to the GIS data, as described in Landi et al. (1999). The GIS spectra have to be *deghosted* (or *reconstructed*), before any scientific use can be made of them. Part of the counts originating from several bright lines are recorded in one or two different regions of the spectrum, thus creating one or two spurious spectral lines, called *ghosts* (see for details: Breeveld 1996; Landi et al. 1999; Del Zanna 1999). In some cases, ghosts appear as

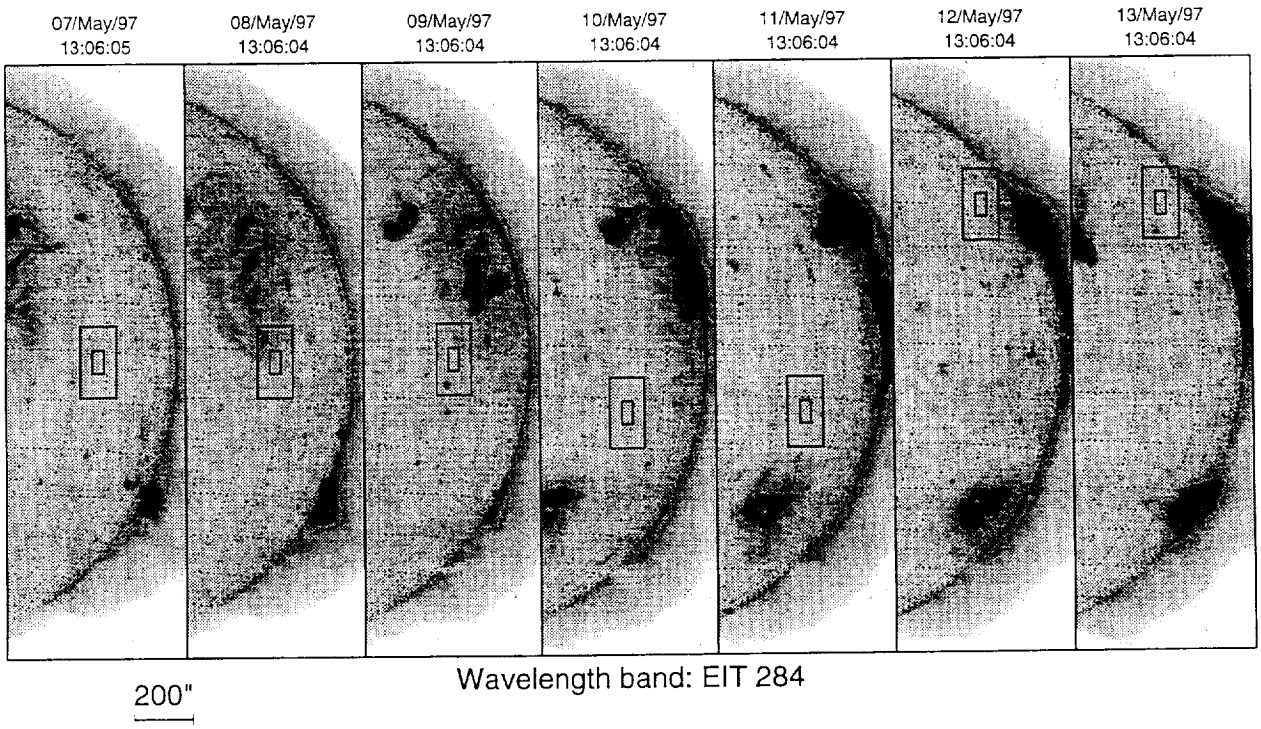

Fig. 3. Areas observed by CDS/NIS (FOV: 120 × 240″) and GIS (FOV: 40 × 80″) during the 7–13 May 1997 JOP16 campaign. The synoptic EIT 284 images shown here were taken near the end of each daily observing sequence.

isolated lines, and the intensities of the lines producing them can be reconstructed. We have followed the method described in Del Zanna et al. (2001), which consists in measuring the line and ghost count rates first, and then reconstruct the GIS spectra. All the features in the GIS spectra (spectral lines identified or not, ghosts) have been considered, for a total of more than 300. A number of second order lines have been identified in the GIS3 and GIS4 spectra (for details, see Del Zanna 1999). These have been removed from the reconstructed spectra. It should be noted that for the quiet Sun observations analysed here the contribution from second order lines to the observed spectra is almost negligible, with the exception of a few lines in the GIS4 spectra (most notably the Mg IX λ368 line), also seen in first order in the NIS spectra. The calibration has been applied as a final step, in order to convert the measured count rates in the NIS and GIS lines to intensities in photons s^{-1} cm^{-2} sr^{-1}.

As a first step, only the line intensities in the brightest lines recorded during the NIS and GIS rasters have been estimated. Monochromatic images of the FOV such as those shown in Fig. 4 have been constructed and inspected in order to judge the time variability and the presence of brightenings. In particular, for each NIS raster, the FOV of the area precedently (or subsequently) observed by GIS has been considered (see Fig. 4), taking into account solar rotation.

A tempting approach to the use of the series of rasters comprising the observing sequence, might involve a detailed analysis of the individual features, in order to carry out the tests described in Sec. 2 on specific quiet-Sun structures, e. g. chromospheric network boundaries and cell center. The rather coarse time resolution of the data series, however, in conjunction with solar rotation, makes this approach very problematic. Furthermore, even if a satisfactory estimate, for instance, of the observed "average" observed coronal photon *intensities* (along the line of sight) over "typical" cell centers were obtained, there would still be the problem of deriving the photon *flux* impinging on the chromosphere from all directions – including the contribution from the surrounding network bright elements. Some additional assumptions about the three-dimensional structure of the atmosphere (chromosphere and corona) would then be necessary.

In the spirit of keeping the number of assumptions to a minimum, in this paper we will only consider average spectra over the co-spatial areas observed by both NIS and GIS throughout each daily sequence, regarded as representative of average quiet Sun conditions. From the 10th of May data a small region with a brightening near the boundary of the GIS FOV has been excluded (see Fig. 4).

For each GIS and NIS raster belonging to a daily observing sequence one average spectrum representing the co-spatial region has been computed. Count rates in the NIS and GIS lines were then obtained with a multiple line profile fitting and removal of a background (see Haugan 1997). Errors on the line intensities were estimated from the errors of the line fitting parameters. Fig. 5 shows the

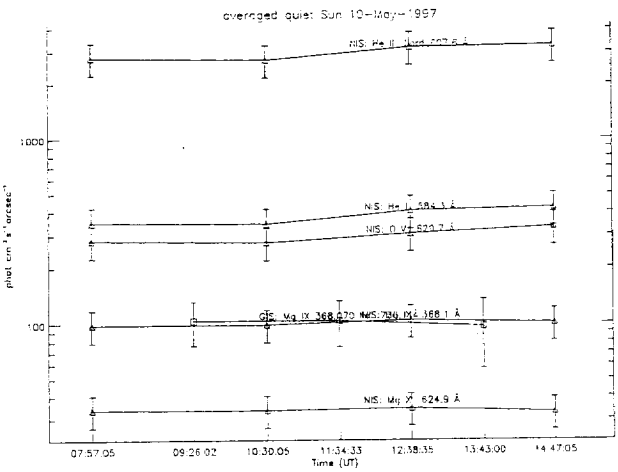

Fig. 5. Time evolution of the calibrated intensities of a few selected lines from the spatially-averaged NIS spectra of the 10th of May (triangles). The Mg IX λ368 line has also been measured in second order in the GIS4 band (squares).

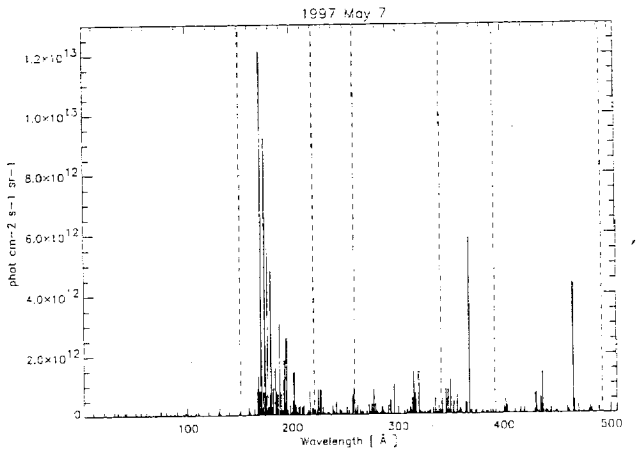

Fig. 6. EUV average spectrum relative to the quiescent region observed on May 7. Lines in the 150–221 Å, 257–340 Å and 384–480 Å ranges are from the average GIS spectrum. Intensities outside the GIS ranges are from CHIANTI theoretical calculations (see Sec. 3.3.1). Note that the strong line in the GIS2–GIS3 gap is the Mg IX λ368 line, observed both in second order GIS4 and first order NIS1 spectra (see also Fig. 5).

time evolution of the calibrated intensities of a few selected lines from the spatially-averaged spectra of the 10th of May. It can be seen that there is little time variability in these averaged intensities. The fact that the calibrated intensity of the Mg IX λ368 line as observed in first (NIS) and second (GIS) order are about the same confirms the validity of the adopted cross-calibration between the two detectors. The omni-present variability of transition region lines such as O V λ630 is smoothed by the averaging over a relatively large area. The data of May 7 also show very little time variability. Once this was established, time-averaged spectra (e. g. one GIS and one NIS spectrum for each day) have been computed, and again count rates obtained with multiple line profile fitting.

3.3.1. Estimation of line intensities outside the observed ranges

As already mentioned, the observed GIS and NIS spectra cover most of the spectral range of interest here ($\lambda < 504$ Å, see Fig. 6). Only four wavelength ranges have incomplete or missing observed data: 1–150 Å; 221–257 Å; 340–384 Å; 480–504 Å. The first range, 1–150 Å, contributes only a small fraction to the total number of photons, as explained below. The second range, 221–257 Å, contains a small number of coronal lines, some of which are observed in second order in the GIS3 detector, plus a few He II lines (the strongest of which is at 256 Å, see discussion in Sec. 3.1). The third range, 340–384 Å, is mostly covered by the NIS1 spectrum in first order (although only a few of the brightest lines have actually been extracted) and by GIS4 in second order. The fourth range, 480–504 Å, only includes a few weak lines.

The 'missing' line intensities have been estimated with theoretical calculations based on the CHIANTI (Dere et al. 1997) atomic database. In particular, version 3.02 (Dere et al. 2001) has been used.

The CHIANTI database has been used by various authors to test the calibration of the SERTS rocket flights and the CDS instrument, and has shown a high degree of accuracy and completeness in the EUV range (see, e. g.: Del Zanna 1999; Del Zanna et al. 2001, and references therein).

We have calculated the line intensities with the assumption of an optically thin collisional plasma, and performing a Differential Emission Measure (DEM) analysis following the method described in Del Zanna et al. (2001). All the observed GIS and NIS line intensities have been considered. They cover a wide range of ions and elements, and allow a good estimate of the DEM from low transition region temperatures ($\log T$ (K) = 4.9; C III, N III) up to high temperatures ($\log T$ (K) = 6.5; Fe XVI, S XIV). Note that the majority of missing lines are emitted in this temperature range.

For the DEM analysis, the line emissivities have been calculated at constant density $n_e = 5 \times 10^8$ cm^{-3}, value derived from the excellent density-sensitive Si X λ347/356 ratio (observed in NIS). It should be noted that the density-sensitive lines missing in these quiet Sun spectra are rather weak, and are mostly emitted in the corona, i. e. around a million degree. The photospheric abundances of Grevesse & Sauval (1998) (with a correction to the oxygen abundance of -0.1 dex, as suggested by recent results, see Allende Prieto et al. 2001) were found to be consistent with the data in all cases. Once a DEM distribution was found, the theoretical intensities of the lines were computed and compared to the observed ones. This procedure allowed a number of useful checks to be performed.

First, we have verified that in all cases the line intensities observed by GIS were consistent (within a 20% or so) with those measured by NIS. This included all the transition region lines (e. g. O III, O V) observed by both instruments, and further confirmed the validity of merging the averaged GIS and NIS data.

Second, we have verified that the computed line intensities of the brightest lines in the missing ranges were in agreement (within 10%) with the measured values. When lines emitted by the same ion are considered, excellent agreement is found, as already shown in Del Zanna et al. (2001). In the other cases, differences are found, but can be explained in terms of uncertainty in the ionization fractions. Considering the missing ranges, a better agreement between theory and observations was found with the use of the old collisional ionization equilibrium computations of Arnaud & Rothenflug (1985), compared to the most recent ones by Mazzotta et al. (1998). We therefore adopted the Arnaud & Rothenflug (1985) calculations. Moreover, for a number of ions the emission measure approach fails in explaining the observed line intensities. This anomalous behaviour is described in detail in Del Zanna (1999) and Del Zanna et al. (2002). Fortunately, these anomalous ions fall in the GIS4 and NIS2 spectra, and not in the missing ranges.

We can therefore be confident that the computed line intensities in the three missing ranges ($\lambda > 150$ Å) are accurate to within 20% or so and are complete.

We now consider the $\lambda < 150$ Å missing range. CHIANTI version 3 (Dere et al. 2001) includes all the relevant ions (e. g. of the H and He isoelectronic sequences) and processes (e. g. inner-shell and satellite lines) that produce spectral lines in the X-ray spectral range (1–150 Å). The coverage in this band can be considerd complete for the purposes of this work, as shown in Del Zanna et al. (2001). We have performed various tests and concluded that the number of photons emitted in this band is a small fraction of the photons recorded by the GIS detectors. This is true even if Active Region (AR) observations are considered. In fact, we have considered as a test case the AR DEM derived by Schmelz et al. (1999) from YOHKOH SXT and SERTS observations. We can be confident that the high-temperature emission measure values are upper limits to the quiet Sun values, and use them at first to constrain the high-T tail of the DEM. However, most of the photons emitted in the 1–150 Å range are produced, even in AR spectra, by ions with peak emission between $\log T$ =6–6.6. The fact that CDS is detecting lines up to $\log T = 6.5$ provides a good constraint on the DEM values at those T and therefore also on most of the photons emitted in the 1–150 Å range.

Moreover, the higher temperature lines mainly affect the shorter wavelengths, while we have shown in Sec. 2.2 that photons below ~ 50 Å would not really matter for our test, because in chromosphere they are mostly absorbed by metals.

The various contributions entering in the estimate of the total coronal emission, including both the observed GIS spectra and the missing lines estimated through the CHIANTI package, are listed in Table 1, for the representative case of the 7 May data. The contributions of EUV continua such as free-free emission and two-photon continua from hydrogenic ions are also listed. The contribution from lines due to ions forming at temperatures below $\log T$ (K) = 5.5 (not listed in the table) is of 4.77×10^{12} photons s^{-1} cm^{-2} sr^{-1}, and is rather small, as expected. The most important thing to note from this table, however, is that GIS spectra do in fact allow a nearly complete count of almost all the photons below 500 Å.

Lines – observed:	
$\Upsilon^{\rm cor}$[GIS1 (150 – 221)]	61.2
$\Upsilon^{\rm cor}$[GIS2 (257 – 340)]	14.7
$\Upsilon^{\rm cor}$[GIS3 (384 – 480)]	21.8
Lines – estimated:	
$\Upsilon^{\rm cor}$[1 – 150]	3.28
$\Upsilon^{\rm cor}$[221 – 228]	3.53
$\Upsilon^{\rm cor}$[228 – 257]	5.95
$\Upsilon^{\rm cor}$[340 – 384]	15.7
$\Upsilon^{\rm cor}$[480 – 504]	0.345
Others:	
$\Upsilon^{\rm free-free}$[1 – 228]	2.73
$\Upsilon^{\rm free-free}$[228 – 504]	4.15
$\Upsilon^{\rm 2-photon}$[1 – 228]	0.627
$\Upsilon^{\rm 2-photon}$[228 – 504]	0.123
Totals:	
$\Upsilon^{\rm cor}[\lambda < 228]$	71.4
$\Upsilon^{\rm cor}[\lambda < 504]$	134.

Table 1. Main contributions to total coronal photoionising intensities, from the 7th of May data. Intensities are in units of 10^{12} photons s^{-1} cm^{-2} sr^{-1}.

3.3.2. Estimation of photon fluxes from observed intensities

The processing of CDS data described so far gives only line-of-sight photon intensities, towards the SOHO spacecraft. With the assumption of optically thin coronal emission, these intensities also give the number of photons per unit solid angle illuminating the chromosphere, from the same direction. On the other hand, a correct application of the tests given by Eqs. 1 and 2 would require the knowledge of the radiation impinging/emitted from/to all directions, averaged over the test surface (Eq. A.17, and Fig. 2).

Since we are considering an average quiet Sun area, we can estimate the contribution from the surrounding corona from the average limb brightening of coronal radiation. If $I(\mu)$ is the average intensity as function of the cosine of the angular distance from disk center, μ, from Eq. A.17 (omitting mention of the frequency band, for brevity) we then have:

$$\Phi^{\rm in} = \frac{2\pi}{h\nu} \int_0^1 \mu\, I(\mu)\, {\rm d}\mu \,. \qquad (3)$$

In terms of observations at a given μ_c:

$$\Phi^{\rm in} = \pi \, f_{\rm cl}(\mu_c) \, \frac{I(\mu_c)}{h\nu} \, , \tag{4}$$

where the correction factor, $f_{\rm cl}(\mu)$, is defined from the center-to-limb variation:

$$f_{\rm cl}(\mu) = 2 \int_0^1 \mu' \, \frac{I(\mu')}{I(\mu)} \, {\rm d}\mu' \, . \tag{5}$$

With this definition the correction factor is unity for a constant $I(\mu)$. An analogous correction factor can be defined for $\Phi^{\rm out}$ as well, from the center-to-limb behaviour of the resonance He lines.

In the case of coronal limb-brightening, apart from some determination from early space missions (e. g.: Withbroe 1970), not much is available in literature. More recent works mostly focus on center-to-limb variations of line widths and/or shifts (e. g.: Thompson & Brekke 2000), or on off-disk measurements. We thus have to resort to SOHO/EIT to estimate the gross properties or coronal emission as a function μ. For such quantitative estimate, we took advantage of recent improvements on the flat-fielding of EIT data (Newmark 2001).

The response of the four EIT filters is centered around 171 Å, 195 Å, 284 Å, and 304 Å. For the first three filters, the main contribution to the observed intensities comes from coronal lines (respectively Fe IX λ171, Fe XII λ195, and Fe XV λ284). The "nominal" temperatures attributed to these images, from the peak of the temperature response, are respectively 1.3×10^6 K, 1.6×10^6 K, and 2.0×10^6 (Delaboudinière et al. 1995), but contributions from other temperatures may be significant, especially for the EIT 195 and EIT 284 bands. The EIT 304 band is usually dominated by the He II λ304; however the Si XI λ303 line may also be important, especially off limb.

Dividing a flat-fielded full-disk EIT image in annuli of constant μ, at each value of μ we can construct an intensity histogram. The result is a two-dimensional histogram such as those shown in Fig. 7. Those histograms show a rather well defined dependence of average intensities with distance from disk center. At this stage of solar activity, with relatively few active regions on the disk, simply finding the mode of the distribution at each value of μ is usually an effective way of filtering out active regions and polar coronal holes, while the width of the central distribution (1-σ, determined from a gaussian fit) provides error bars. In Fig. 7 we show the two-dimensional histogram of only one of the coronal EIT bands (EIT 171). Note below the main quiet-Sun distribution at $\mu < 0.4$, in the EIT 171 and (somewhat less distinct) in the EIT 304 histograms, the distribution corresponding to the polar coronal holes. Histograms from the other two coronal bands do not add much information, except for a somewhat greater signature of active regions at the corresponding disk-center distances.

In the case of the coronal filter, we have superimposed a curve obtained from a very simple model of emissivity exponentially stratified with a scale height, H, computed for a H+He fully ionised plasma: $H = kT/wm_{\rm H}g_\odot$

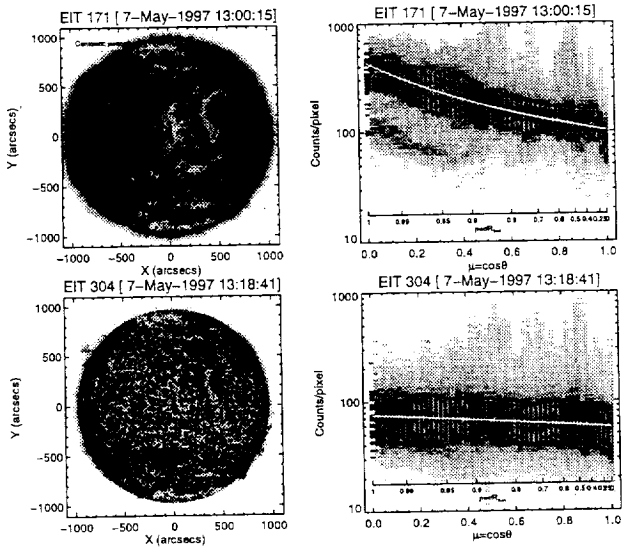

Fig. 7. Synoptic EIT images (left panels) and corresponding two-dimensional histograms intensity vs. μ (right panels). In the two-dimensional histograms, the mode and width of the distribution at each value of μ are indicated by points with error bars, while the solid lines show the fits to these values, as described in Sec. 3.3.2.

($w = 0.59$ is the plasma mean molecular weight, $m_{\rm H}$ is the mass of the hydrogen atom, and $g_\odot$ is the solar surface gravity). Assuming an optically thin plasma, and thus from simple geometrical considerations, the resulting intensities integrated along the line of sight are:

$$I(\mu, T) \propto \int_0^\infty {\rm d}x \exp\left\{ -\frac{R_\odot}{H(T)} \left(\sqrt{1 + 2x\mu + x^2} - 1 \right) \right\} . \tag{6}$$

In Eq. 6 we used the "nominal" temperature of the filter, while the proportionality constant has been determined for each image by minimising the weighted χ^2.

In the case of the EIT171 filter, shown in Fig. 7, the simple isothermal model given by Eq. 6 seems to give an adequate representation of the "average" properties of the on-disk quiet corona, at least for the purpose of justifying its use in Eq. 5. The results for the other two coronal bands, not shown here, are not too dissimilar, despite their filter temperature response being much less accurately represented by an isothermal approximation.

The correction factors given by inserting Eq. 6 in Eq. 5 are only weakly dependent on the assumed value of $H(T)$. We adopt here as a representative temperature of the lines in the GIS range the value $T = 1.0 \times 10^6$ K, obtained from an intensity-weighted average of the temperatures of observed GIS lines. The correction factors corresponding to $\mu_c = 0.64$ and $\mu_c = 0.66$ are, respectively, $f_{\rm cl} = 1.06$ and 1.09.

In the case of the EIT 304 band, we compared the center-to-limb variation shown in Fig. 7 with the dependence found by Mango et al. (1978):

$$I(\mu) \propto 1 + a \, (1 - \mu) \tag{7}$$

	07-May-1997	10-May-1997
μ_c	0.66	0.64
Coronal radiation:		
$\Upsilon^{cor}[\lambda < 228]$	71.4	74.2
$\Upsilon^{cor}[\lambda < 504]$	134.	132.
f_{cl}^{cor}	1.09	1.063
$\Phi^{cor}[\lambda < 228]$	77.8	78.9
$\Phi^{cor}[\lambda < 504]$	146.	140.
Helium radiation:		
Υ^{res}[He I λ584]	15.8	16.1
f_{cl}^{res}[He I λ584]	1.0	0.998
Υ^{res}[He I λ537]	1.38	1.49
f_{cl}^{res}[He I λ537]	0.997	0.990
Υ^{res}[He II λ304]	115.	127.
f_{cl}^{res}[He II λ304]	0.998	0.993
Φ^{res}[He I]	>17.2	>17.5
Φ^{res}[He II]	>115.	>126.
Φ^{res}[He]	>132.	>144.

Table 2. Photon intensities and fluxes from the three data sets discussed in this paper. Same units as in Table 1. The conversion factors from intensities to fluxes, f_{cl}, derived as described in Sec. 3.3.2, are also listed. As discussed in the text, the tabulated helium photon fluxes are only lower limits to Φ^{res}[He I] and Φ^{res}[He II].

with $a = 0.31$ for the He II λ304 in the the quiet Sun (again, the scale factor has been found by fitting the data). For the He I λ584 and He I λ537, Mango et al. (1978) give $a = 0.10$ and $a = 0.47$, respectively.

From Eq. 7, the correction factor is $f_{cl} = (1+a/3)/[1+a\,(1-\mu_c)]$. The values of f_{cl} are practically unity within 1%, for the actual values μ_c of the observations analysed here (which are very near $\mu = 2/3$), and for the values of a given for the resonance He lines we are considering. In fact, at $\mu = 2/3$, we would have $f_{cl} = 1$ regardless of the value of a. Therefore, any contamination due to the Si XI λ303 line both in the Skylab data analysed by Mango et al. (1978) and in the broad-band EIT 304 images would not significantly affect this result, as long as a linear relationship as in Eq. 7 still fits the data.

Analogously, we note that if the correction factors for Φ^{cor} are nearly unity, it is also because of the particular location of the rasters we have considered (at $\mu_c \sim 2/3$). Had we considered observations at disk center, the correction factor would have been $f_{cl} = 1.54$ for the coronal lines, while still being close to unity for Φ^{He} (1.10, 1.03, and 1.16 for He II λ304, He I λ584, and He I λ537, respectively) – because of the flat center-to-limb dependence of the helium resonance lines. Conversely, the coronal correction factor for the 12 and 13 May observations (at $\mu_c \sim 0.4$), would have been 0.74.

3.4. Results

Table 2 lists the results of the analysis described in Sec. 3.3. Both the total observed intensities, Υ, and the flux conversion factors, f_{cl}, are listed, together with the final result: the photon fluxes required by Eqs. 1 and 2.

As mentioned in Sec. 3.3, we estimate the relative accuracy of the GIS and NIS observed intensities to be within 20%. This is the main uncertainty in the comparison between Φ^{res}[He] and Φ^{cor}.

However, while the estimate of the total photon fluxes in the bands $\lambda < 504$ and $\lambda < 228$ are essentially complete, helium photon fluxes are only lower limits to the total fluxes Φ^{res}[He], because of the missing contributions from all higher resonance lines and, probably more important, from the resonance recombination continua.

Therefore, the test of Eq. 1 applied to the 7 May data is satisfied only if the missing contribution to Φ^{res}[He] is below 30%. For the 10 May data, where Φ^{res}[He] is already higher than $\Phi^{cor}[\lambda < 504]$, the missing contribution must be correspondingly smaller (less than 15%). From the discussion of Sec. 3.1, this seems rather unlikely. Furthermore, no loss of photons in the P-R process due to background absorbers is allowed. From the considerations of Sec. 2.2, this in practice means that hydrogen, the main background absorber at those wavelengths, should be completely ionised in the P-R layer. Once more, this is a rather strong requirement, if we consider that the P-R layer is expected to be located in the upper chromosphere.

Application of the test given by Eq. 2 yields much more clear-cut results: the intensity of the He II λ304 alone is about 50% higher than the total photon flux in the range $\lambda < 228$ Å. Thus, the hypothesis that the He II EUV emission is entirely due to the P-R mechanism is to be rejected.

We note at this point that the results of these two tests do no allow us to say much about the formation mechanism of the He I EUV spectrum. But, if we consider He II emission – however produced – as another source of photoionisation for He^0, the observed He I EUV emission becomes compatible with a P-R formation: Φ^{res}[He I] < Φ^{res}[He II] + $\Phi^{cor}[\lambda < 504]$, by more than an order of magnitude. We recall however (see App. A) that such a straightforward comparison can be done only if we can assume that He II photoionising emission takes place *above* the P-R layer where the He I spectrum is produced. The more realistic case of nearly co-spatial He I and He II emission would, on the other hand, require a more detailed treatment of the transfer of radiation.

In comparison with these quiet Sun data, the data from the 11 May brightening indicate an even more significant excess of He emission, compared with coronal radiation, both for the total Φ^{res}[He I]+Φ^{res}[He II] radiation, and for the He II λ304 alone. We obtain, respectively: $\Upsilon^{cor}[\lambda < 228] = 1.14 \times 10^{14}$, $\Upsilon^{cor}[\lambda < 504] = 2.15 \times 10^{14}$, Υ^{res}[He I λ584] $= 3.60 \times 10^{13}$, Υ^{res}[He I λ537] $= 3.03 \times 10^{12}$, and Υ^{res}[He II λ304] $= 2.59 \times 10^{14}$ photons s^{-1} cm^{-2} sr^{-1}. It would be interesting (and we plan to investigate this point in the future) to verify whether this result can be extrapolated to more active areas of the solar atmosphere.

Finally, we also examined with the same criterion data for the well studied 1996 "Elephant's Trunk" coronal hole (Del Zanna & Bromage 1999). In coronal holes,

both He and coronal EUV radiation are strongly suppressed, but the latter to a greater extent (even a simple visual inspection of Fig. 7 shows this). In fact, considering intensities only, we obtained that $\Upsilon^{\rm res}$[He] exceeds $\Upsilon^{\rm cor}[\lambda < 504]$ by more than a factor 2, while $\Upsilon^{\rm res}$[He II] exceeds $\Upsilon^{\rm cor}[\lambda < 228]$ by more than a factor 4. There is little doubt in this case that the P-R mechanism is not playing a significant role in the excitation of the helium spectrum in coronal holes.

4. Conclusions

The results presented in this paper indicate quite clearly that the excitation of the EUV helium spectrum in the quiescent solar atmosphere cannot be explained solely by a simple photoionisation-recombination process induced by coronal emission – the so-called P-R mechanism. More specifically, the observed coronal EUV flux cannot explain the formation of the He II λ304 via the P-R mechanism. We consider this conclusion quite robust, given the minimum number of assumptions involved in the tests performed.

The data discussed here refer to quiescent areas, for the Sun near its minimum of activity. We have also discussed a small network brightening, drawing an analogous conclusion. Likewise, we were able to extend these results to the case of a coronal hole. It becomes now of foremost interest the possibility of performing a similar analysis in active regions: we plan to examine existing SOHO archive data in order to carry out the tests described in this paper.

On the other hand, our results do not give a definite answer regarding the formation of the He I spectrum without further assumptions. If we can assume that He II resonance emission – the He II λ304 in particular – is produced by some other mechanism in higher layers of the atmosphere, the observed He I intensities are well compatible with a P-R process acting in the chromosphere, in the sense that it verifies inequalities such as Eq. A.18. The tendency of observed He I λ584 structures to match very closely those seen in He II λ304 images (Macpherson & Jordan 1999), would even indicate that the formation of the He I spectrum is in fact dominated, via the P-R mechanism, by the latter line flux. However, from Table 2 it seems that the He II λ304 line does indeed give an important contribution to the total flux below 504 Å, but is by no means completely dominant. Hence, we would expect the He I λ584 line to show some correlation with coronal images as well, and that would likely degrade the excellent obseved correlation with the He II λ304 line. Moreover, there are other observational constraints – such as observed line profiles, ratio He I λ584/He I λ537, color temperature of the resonance continuum (for a more in-depth discussion, see Andretta & Jones 1997) – which are less compatible with a spectrum formation dominated by the P-R mechanism. At this stage, we can only say that the problem of the formation of the He I spectrum is, if possible, even more open than the problem of the formation of the He II lines.

A possible approach to this problem requires more sophisticate modelling, including the radiative interaction between He II λ304 and He I lines. To this respect, we note that various authors in the past (e. g.: Fontenla et al. 1993; Wahlstrøm & Carlsson 1994) have performed rather detailed calculations, concluding that the He II λ304 line is not very important in the photoionisation of He I in the solar atmosphere. We find these arguments not very convincing: the He II λ304 intensities computed by those authors are always much lower (even by an order of magnitude) than the observed values. Using the observed He II λ304 intensities could significantly alter the picture.

In any case, we remark that the results presented here refer only to the resonance spectrum, i. e. only to the EUV lines. The subordinate spectrum, whose lines and continua have vastly lower optical depths, may as well be described by the P-R mechanism, or by a mixture of collisional and P-R excitation (as discussed, e. g., by Andretta & Jones 1997, in the case of He I).

Moreover, the hypothesis we have tested is that the P-R mechanism is the *dominant* mechanism in the formation of the He spectrum. The fact that this hypothesis has been rejected does not exclude that the P-R mechanism could give a significant contribution to the total intensities of the He EUV lines.

If we assume, for the sake of argument, that about 1/2 of the $\lambda < 504$ photons in the P-R mechanism are emitted in the resonance continua (see Sec. 3.1) and assuming that about 1/2 of the photons are absorbed by hydrogen atoms (see Sec. 2.2), from the values of $\Phi^{\rm cor}[\lambda < 504]$ of Table 2 a possible estimate for the P-R contribution would be about 1/4 of the observed flux $\Phi^{\rm res}$[He]. A similar estimate based on the ratio between $\Phi^{\rm cor}[\lambda < 228]$ and $\Phi^{\rm res}$[He II] would imply a P-R contribution of the order of 15%. We stress that these may not even be order-of-magnitude estimates, but just examples based on some, not necessarily realistic assumptions on the transfer of EUV coronal and helium radiation and on the ionisation equilibrium of helium and hydrogen in the solar chromosphere. More precise estimates would require detailed numerical NLTE calculations in model solar chromospheres.

However, two comparable, but dynamically weakly coupled components (one formed in the chromosphere and the other in the TR) should leave some signature in helium line profiles, especially in the relatively frequent events involving considerable line shifts in TR lines. We are not aware of any reports of multiple components in helium lines which could be unambiguously interpreted as a dynamical TR component superimposed on a chromospheric, P-R component.

Finally, the fact that the P-R mechanism is definitely not the dominant formation mechanism for the He II λ304 line and, perhaps, for the resonance He I spectrum, calls for renewed attempts to propose a credible alternative mechanism, considering that current methods applied to current solar model atmospheres fail badly to reproduce the observed intensities (e. g.: Fontenla et al. 1993; Macpherson & Jordan 1999). Albeit formulated in a rather coarse and

semi-qualitative form, the V-R mechanism first proposed by C. Jordan (1975), and more recently further developed by Andretta et al. (2000), seems to be, in our opinion, on the right track. Investigations of the effects of non-thermal electrons were initially promising for the helium spectrum, although failing to simultaneously reproduce all the other UV emission lines (Anderson et al. 1996). However, more recent studies (G. Smith 2001) have given much less encouraging results even for the He lines. Nevertheless, we must note that the possibility of helium abundance variations in the solar atmosphere has rarely considered as a possible explanation. This is perhaps suprising, especially in consideration of the strong variations of helium abundance observed in the solar wind. It is true that some theoretical models (Hansteen & Leer 1997) would rather predict a depletion of helium in the TR, instead of the required strong enhancement, but the physics of such effects is sufficiently complex to merit further investigations, both on the observational and on the theoretical side.

Acknowledgements. Part of this work was carried out while one of the authors (V. A.) held a National Research Council–NASA Research Associateship at Goddard Space Flight Center. V. A. also acknowledges partial funding from NASA/GSFC Grant NCC 5-377.

G. D. Z. acknowledges support from PPARC (UK) and MIUR (Italy).

We thank the staff of NASA's National Space Science Data Center for their support in obtaining the Fortran routines used to compute low-energy X-ray metal cross-sections shown in Fig. 1.

We are grateful to Jeff Newmark for providing the calibrated SOHO/EIT images used in Sec. 3.3.2.

SOHO is a project of international cooperation between NASA and ESA.

Appendix A: Photoionisation-recombination process in a semi-infinite, cool atmosphere

We start off with writing the equation of radiative transfer[2] averaged over all directions:

$$\boldsymbol{\nabla}\cdot\boldsymbol{F}_\nu = -\chi_\nu J_\nu + \eta_\nu, \tag{A.1}$$

where χ_ν and η_ν are the monochromatic absorption and emission coefficients, respectively, J_ν is the mean intensity: $J_\nu = (4\pi)^{-1}\int I_\nu \mathrm{d}\Omega$, and $\boldsymbol{F}_\nu$ is the flux: $\boldsymbol{F}_\nu = (4\pi)^{-1}\int \boldsymbol{n} I_\nu \mathrm{d}\Omega$ ($\boldsymbol{n}$ is the unit vector specifying the direction towards the solid angle $\mathrm{d}\Omega$). In writing Eq. A.1 we have assumed that opacity and emissivity are isotropic.

The opacity and emissivity due the radiative transition between levels i and j of an atomic system ($i < j$, if we index levels with increasing energy) are:

$$\chi_{ij} = n_i\sigma_{ij}(\nu), \tag{A.2}$$

$$\eta_{ij} = n_j\sigma_{ji}(\nu)\,(J_\nu + 2h\nu^3/c^2). \tag{A.3}$$

[2] Notations and conventions mostly from Mihalas (1978), except that we do not include stimulated emission in the absorption coefficient as a negative opacity term.

For bound-bound transitions, the cross-sections σ include the absorption/emission profiles (whichever applies); n_i is the population per unit volume of atomic level i. For bound-bound transitions with complete redistribution in frequency, or for bound-free continua, we have: $\sigma_{ji}(\nu) = \sigma_{ij}(\nu)(n_i/n_j)^*\exp(-h\nu/kT)$, where $(n_i/n_j)^*$ is the ratio of the (Saha-)Boltzmann populations.

For every photon absorbed or emitted by the atom, there corresponds a radiative transition. Thus, using Eqs. A.2 and A.3, we can write the radiative excitation/ionisation and decay/recombination rates as:

$$n_i R_{ij} = \int_{\Delta\nu_{ij}} \frac{4\pi}{h\nu}\chi_{ij}(\nu)J_\nu \mathrm{d}\nu, \tag{A.4}$$

$$n_j R_{ji} = \int_{\Delta\nu_{ij}} \frac{4\pi}{h\nu}\eta_{ij}(\nu)\mathrm{d}\nu, \tag{A.5}$$

where $\Delta\nu_{ij}$ is the relevant frequency range for the given transition ($\nu >$ threshold, for a continuum; the width of the line, for a bound-bound transition).

For a line or continuum not overlapping with other transition of the same atomic system, we can then multiply Eq. A.1 by $4\pi/h\nu$ and integrate over $\Delta\nu_{ij}$ to obtain:

$$\boldsymbol{\nabla}\cdot\boldsymbol{\Phi}[\Delta\nu_{ij}] = -n_i R_{ij} + n_j R_{ji} - \int_{\Delta\nu_{ij}} \frac{4\pi}{h\nu}\left[\chi_b(\nu)J_\nu - \eta_b(\nu)\right]\mathrm{d}\nu, \tag{A.6}$$

where χ_b and η_b are the contribution to opacity and emissivity, respectively, from sources different from the atomic system under consideration ("background" opacity/emissivity). In Eq. A.6, the quantity $\boldsymbol{\Phi}[\Delta\nu]$ is the total photon flux, integrated over all the directions and over the frequency band $\Delta\nu$:

$$\boldsymbol{\Phi}[\Delta\nu] \equiv \int_{\Delta\nu} \frac{4\pi}{h\nu}\boldsymbol{F}_\nu \mathrm{d}\nu = \int_{\Delta\nu}\mathrm{d}\nu\int \mathrm{d}\Omega\,\boldsymbol{n}\frac{I_\nu(\boldsymbol{n})}{h\nu}. \tag{A.7}$$

Less important in this discussion, but nevertheless useful from an observational point of view, is the total photon intensity integrated on the band $\Delta\nu$ along the direction $\boldsymbol{n}$; we therefore introduce a special notation for this quantity too:

$$\Upsilon[\Delta\nu](\boldsymbol{n}) \equiv \int_{\Delta\nu}\mathrm{d}\nu\,\frac{I_\nu(\boldsymbol{n})}{h\nu}. \tag{A.8}$$

Finally, for the remainder of the discussion, it is also convenient to abbreviate the notation for the "background" contribution:

$$\mathrm{bg}[\Delta\nu] \equiv \int_{\Delta\nu} \frac{4\pi}{h\nu}\left[\chi_b(\nu)J_\nu - \eta_b(\nu)\right]\mathrm{d}\nu. \tag{A.9}$$

If transition $i \longleftrightarrow j$ overlaps with another transition of the same atom or element, $h \longleftrightarrow k$, we can still write an equation similar to Eq. A.6:

$$\boldsymbol{\nabla}\cdot\boldsymbol{\Phi}[\Delta\nu_\cup] = -n_i R_{ij} - n_h R_{hk} + n_j R_{ji} + n_k R_{kh} - \mathrm{bg}[\Delta\nu_\cup], \tag{A.10}$$

where now the integration is carried out over the set of frequencies covering both transitions: $\Delta\nu_\cup \equiv \Delta\nu_{ij} \cup \Delta\nu_{hk}$.

So far, we have merely introduced some notations, and re-formulated the equation of transfer (the only assumption was the isotropy of the absorption and emission coefficients). We now introduce the equations of statistical equilibrium to express the sources and sinks of photons in terms of collisional rates.

For instance, we consider the example of an ion with N bound levels (ground level indexed with 0) plus continuum. A count of all recombining photons is given by summing Eq. A.6 for the resonance lines and the direct recombination continuum; with the adoption of the notation $\Delta\nu_\cup \equiv \bigcup_i \Delta\nu_{0i}$, we have:

$$\boldsymbol{\nabla}\cdot\boldsymbol{\Phi}[\Delta\nu_\cup] = -n_0\sum_i R_{0i} + \sum_i n_i R_{i0} - \mathrm{bg}[\Delta\nu_\cup]. \quad \text{(A.11)}$$

With the introduction in Eq. A.11 of the statistical equilibrium equations, we can then write:

$$\boldsymbol{\nabla}\cdot\boldsymbol{\Phi}[\Delta\nu_\cup] = +n_0\sum_i C_{0i} - \sum_i n_i C_{i0} - \mathrm{bg}[\Delta\nu_\cup], \quad \text{(A.12)}$$

where C_{ij} are the collisional transition rates.

Another example is an extremely simplified 6-level model for the He ionic system: levels He^0 $1s^2\,{}^1\mathrm{S}$, $1s2s\,{}^3\mathrm{S}$ and $1s2p\,{}^1\mathrm{P}$ (levels 0, 1 and m), levels He^+ $1s$ and $2p$ (levels 2 and 3), and He^{++} (level 4). Transitions $2 \longleftrightarrow 3$ ($\lambda = 304$ Å) and $2 \longleftrightarrow 4$ ($\lambda < 228$ Å) overlap with transition $0 \longleftrightarrow 1$ ($\lambda < 504$ Å). While by no means realistic, this example illustrates the case of overlapping transitions in the presence of a metastable level. The wavelength range we need to consider to account for all the recombinations, $\Delta\lambda_\cup$, includes the range $\lambda < 504$ Å (which covers the two continua and He II λ304), and the wavelengths covering the profile of He I λ584:

$$\boldsymbol{\nabla}\cdot\boldsymbol{\Phi}[\lambda584] = n_1R_{10} - n_0R_{01} - \mathrm{bg}[\lambda584] \quad \text{(A.13)}$$

$$\boldsymbol{\nabla}\cdot\boldsymbol{\Phi}[\lambda<504] = n_2R_{20} - n_0R_{02} + n_3R_{32} - n_2R_{23} + n_4R_{42} - n_2R_{24} - \mathrm{bg}[\lambda<504]. \quad \text{(A.14)}$$

Summing Eqs. A.13 and A.14, and using the equations of statistical equilibrium, we then obtain:

$$\boldsymbol{\nabla}\cdot\boldsymbol{\Phi}[\Delta\nu_\cup] = n_0C_{01} - n_1C_{10} + n_0C_{02} - n_2C_{20} + n_2C_{23} - n_3C_{32} + n_2C_{24} - n_4C_{42} + n_0C_{0m} - n_mC_{m0} - \mathrm{bg}[\Delta\nu_\cup]. \quad \text{(A.15)}$$

Integrating the above equations over a volume V, bounded by surface S, we can express the photon flux across S in terms of the total number of emitted or absorbed photons in the volume. Of course, these terms still depends, explicitly or implicitly, on the radiation field, so we have not really gained anything in the solution of the full non-LTE radiative problem. However, if we assume that when integrated in the volume V:

1. the collisional *excitation* and *ionisation* terms are negligible ($C_{0i} \approx 0$ in the first example, Eq. A.12, or C_{01}, C_{02}, C_{0m}, C_{23} and $C_{24} \approx 0$ in Eq. A.15);
2. the background *emission* is negligible ($\eta_b(\nu) \approx 0$: hence $\mathrm{bg}[\Delta\nu_\cup] \geq 0$);

so that only sinks of photons remain in the right-hand sides of the above relations, we then have:

$$\iint_S \boldsymbol{\Phi}[\Delta\nu_\cup]\cdot\mathrm{d}\boldsymbol{S} \leq 0. \quad \text{(A.16)}$$

The key point is now the choice of the boundary conditions, which depend of course on the physics and geometry of the problem. In a semi-infinite atmosphere (as in the case of the solar P-R chromospheric layer), it is convenient to separate the flux of Eq. A.16 in fluxes through the boundary surfaces above and below the layer, as in Fig. 2 (surfaces S' and S'', respectively).

Thus, surface S'' can be placed in a region where all incident photons have all been either destroyed by collisional processes or re-emitted back (perhaps after multiple absorption/re-emissions or scattering processes) through surface S'. We also assume that the emission of the "cool" atmosphere below the P-R layer is negligible at the frequencies we are considering – as it would be the case of the far EUV emission from the photosphere of a late-type star – and we choose to consider a volume whose dimensions in the horizontal directions are much larger than in the vertical direction, so that we can neglect side contributions. Therefore, the largest contribution to the surface integral in Eq. A.16 comes from the flux through surface S'.

We then divide the latter term in "incoming" and "outgoing" average photon flux:

$$\Phi^{\mathrm{in,out}}[\Delta\nu] \equiv \frac{1}{S'}\int_{\Delta\nu}\iint_{S'}\int_{\mu<,>0}\mathrm{d}\nu\,\mathrm{d}\Omega\,\mathrm{d}S\,|\mu|\frac{I_\nu(\boldsymbol{n})}{h\nu}, \quad \text{(A.17)}$$

where μ is the cosine of the angle between $\boldsymbol{n}$ and $\mathrm{d}\boldsymbol{S}$, obtaining finally:

$$\Phi^{\mathrm{out}}[\Delta\nu_\cup] \leq \Phi^{\mathrm{in}}[\Delta\nu_\cup]. \quad \text{(A.18)}$$

The equality in relations A.16 and A.18 holds only if *all* collisional and background terms (not just ionisation/excitation rates and emissivities) are zero. In this case, the atmosphere re-emits back the same number of incident photons (a direct implication, in fact, of the adopted boundary conditions at S''), though, in general, with a different spectral distribution, as determined by the details of the transport of radiation and of the atomic structure.

References

Allende Prieto, C., Lambert, D. L., & Asplund, M. 2001, ApJ, 556, L63

Anderson, S. W., Raymond, J. C., & van Ballegooijen, A. 1996, ApJ, 457, 939

Andretta, V. 1994, PhD thesis, Univ. of Naples "Federico II" (Italy)

Andretta, V. & Jones, H. P. 1997, ApJ, 489, 375
Andretta, V., Jordan, S. D., Brosius, J. W., Davila, J. M., Thomas, R. J., Behring, W. E., & Thompson, W. T. 2000, ApJ, 535, 438
Arnaud, M. & Rothenflug, R. 1985, A&AS, 60, 425
Athay, R. G. 1988, ApJ, 329, 482
Bałucińska-Church, M. & McCammon, D. 1992, ApJ, 400, 699
Breeveld, A. A. 1996, PhD thesis, Univ. of London (UK)
Breeveld, A. A., Edgar, M. L., Smith, A., Lappington, J. S., & Thomas, P. D. 1992, Rev. Sci. Instr., 63, 1
Brekke, P., Thompson, W. T., Woods, T. N., & Eparvier, F. G. 2000, ApJ, 536, 959
Brosius, J. W., Davila, J. M., & Thomas, R. J. 1998, ApJS, 119, 255
Chapman, S. 1931, Proc. Phys. Soc, 43, 26
Del Zanna, G. 1999, PhD thesis, Univ. of Central Lancashire (UK)
Del Zanna, G. & Bromage, B. J. I. 1999, J. Geophys. Res., 104, 9753
Del Zanna, G., Bromage, B. J. I., Landi, E., & Landini, M. 2001, A&AS, 379, 708
Del Zanna, G., Dere, K. P., Landi, E., Landini, M., Mason, H. E., & Young, P. R. 2001, in ASP Conf. Ser., Vol. 234, X-ray Astronomy 2000, ed. R. Giacconi, S. Serio, & L. Stella (San Francisco: ASP)
Del Zanna, G., Landini, M., & Mason, H. E. 2002, A&A, 385, 968
Delaboudinière, J.-P. et al. 1995, Sol. Phys., 162, 291
Dere, K. P., Landi, E., Mason, H. E., Monsignori Fossi, B. C., & Young, P. R. 1997, A&AS, 125, 149
Dere, K. P., Landi, E., Young, P. R., & Del Zanna, G. 2001, ApJS, 134, 331
Domingo, V., Fleck, B., & Poland, A. I. 1995, Sol. Phys., 162, 1
Falconer, D. A., Jordan, S. D., Brosius, J. W., Davila, J. M., Thomas, R. J., Andretta, V., & Hara, H. 1998, Sol. Phys., 180, 179
Fontenla, J. M., Avrett, E. H., & Loeser, R. 1993, ApJ, 406, 319
Grevesse, N. & Sauval, A. J. 1998, Space Sci. Rev., 85, 161
Hansteen, V. H. & Leer, E. 1997, ApJ, 482, 498
Harrison, R. A. et al. 1995, Sol. Phys., 162, 233
Haugan, S. V. H. 1997, The Component Fitting System for IDL, CDS Software Note 47, http://solg2.bnsc.rl.ac.uk/swnotes/cds_swnote_47.ps
Henke, B. L., Lee, P., Tanaka, T. J., Shimabukuro, R. L., & Fujikawa, B. K. 1982, Atomic Data and Nuclear Data Tables, 27, 1
Huber, M. C. E. et al., eds. in press, The Radiometric Calibration of SOHO, ISSI Scientific Report
Jordan, C. 1975, MNRAS, 170, 429
Jordan, C. 1980, Phil. Trans. R. Soc. London, Ser. A, 297, 541
Jordan, S. D., Thompson, W. T., Thomas, R. J., & Neupert, W. M. 1993, ApJ, 406, 346
Karzas, W. J. & Latter, R. 1961, ApJS, 6, 167
Landi, E., del Zanna, G., Breeveld, E. R., Landini, M., Bromage, B. J. I., & Pike, C. D. 1999, A&AS, 135, 171
Landini, M. & Monsignori Fossi, B. C. 1990, A&AS, 82, 229
Macpherson, K. P. & Jordan, C. 1999, MNRAS, 308, 510
Mango, S. A., Bohlin, J. D., Glackin, D. L., & Linsky, J. L. 1978, ApJ, 220, 683
Mazzotta, P., Mazzitelli, G., Colafrancesco, S., & Vittorio, N. 1998, A&AS, 133, 403
McCammon, D. & Morrison, R. 1983, ApJ, 270, 119
Mihalas, D. 1978, Stellar Atmospheres, 2nd edn. (San Francisco: Freeman)
Newmark, J. 2001, private communication
Schmelz, J. T., Saba, J. L. R., Strong, K. T., Winter, H. D., & Brosius, J. W. 1999, ApJ, 523, 432
Smith, G. 2001, PhD thesis, Univ. of Oxford (UK)
Thomas, R. J. 2001, private communication
Thomas, R. J., Davila, J. M., Thompson, W. T., Kent, B. J., & Hollandt, J. 1999, in American Astronomical Society Meeting, Vol. 194, 1606
Thomas, R. J. & Neupert, W. M. 1994, ApJS, 91, 461
Thompson, W. T. 2001, private communication
Thompson, W. T. & Brekke, P. 2000, Sol. Phys., 195, 45
Vernazza, J. E., Avrett, E. H., & Loeser, R. 1981, ApJS, 46, 635
Vernazza, J. E. & Reeves, E. M. 1978, ApJS, 37, 485
Wahlstrøm, C. & Carlsson, M. 1994, ApJ, 433, 417
West, J. B. & Marr, G. V. 1976, Proc. R. Soc. London A, 349, 397
Wilhelm, K. et al. 1995, Sol. Phys., 162, 189
Withbroe, G. L. 1970, Sol. Phys., 11, 42
Zirin, H. 1975, ApJ, 199, L63
—. 1988, Astrophysics of the Sun (Cambridge: Cambridge Univ. Press)